Enhancements of the Andreev conductance due to emission/absorption of bosonic quanta

Enhancements of the Andreev conductance due to emission/absorption of bosonic quanta

J Barański[1,2] and T Domański[1]

[1] Institute of Physics, M. Curie-Skłodowska University, 20-031 Lublin, Poland
[2] Institute of Physics, Polish Academy of Sciences, 02-668 Warsaw, Poland

E-mail: doman@kft.umcs.lublin.pl

CrossMark

Abstract

We predict that the subgap spectrum and transport properties of the quantum dot embedded between superconducting and metallic reservoirs can be substantially enhanced by emission/absorption of external bosonic quanta. Upon tuning the gate voltage the in-gap Andreev states eventually interfere with each other. We explore the measurable signatures of such interference appearing in the differential conductance for both linear and nonlinear regimes.

Keywords: Andreev scattering, in-gap states, quantum interference

(Some figures may appear in colour only in the online journal)

1. Introduction

Numerous theoretical studies have shown that bosonic modes, such as photons [1] or vibrational degrees of freedom [2, 3], strongly affect electron transport through nanoscopic systems [4–6]. When level spacing of a nano-object is large in comparison to the boson energy ω_0 and line broadening is sufficiently narrow, a series of side-peaks (spaced by ω_0) [7] appear, caused by emission/absorption of the bosonic quanta. These features have been indeed observed in the differential conductance of various nanoscopic structures [8–12].

The role of bosonic modes is currently also of interest in systems comprising quantum dots coupled to superconducting reservoirs. Since the proximity effect spreads electron pairing onto the quantum dots, the bosonic features manifest themselves in a very peculiar way. The influence of such modes has already been addressed in the context of Josephson [13–20] and Andreev spectroscopy [21–26]. Closely related issues have been studied regarding photon-assisted tunneling [27] and transient phenomena [28]. Absorption of boson (vibron or photon) quanta in Andreev scattering may even find some practical applications, e.g. in prototypes of nanoscopic refrigerators [29]. This subgap Andreev current enables construction of nanoscopic thermometers that do not produce any self-heating [30]. In more complex three-terminal hybrid devices (consisting of two metallic electrodes and one superconducting lead) the subgap transport allows separation of charge from heat currents [31], production of spatially entangled (de-paired) electrons [32, 33], realization of exotic Majorana or Weyl quasiparticles, and many other interesting phenomena.

We shall study here the in-gap (Andreev) states and their influence on subgap transport for the hybrid junction shown in figure 1. For $\omega_0 \ll \Delta$ (where Δ is the energy gap of the superconducting electrode), a number of the bosonic features are doubled (in a subgap regime) because of the proximity effect that mixes the particle and hole excitations. Several authors [21, 25, 29] have indicated (numerically) that the subgap conductance is enhanced by the bosonic mode as a function of the gate voltage—these enhancements show up with an intriguing period $\omega_0/2$. To our knowledge, such a theoretical prediction has been not clarified on any physical grounds (we propose to explain this effect). As regards its empirical verification, this should be feasible using either the low-frequency vibrations of some heavy molecules or the slowly-varying ac electromagnetic field. We emphasize that such a low-energy boson mode does not have to be related to any pairing mechanism in the superconducting reservoir.

For microscopic calculations we consider the generic scheme displayed in figure 1. It can be realized practically in
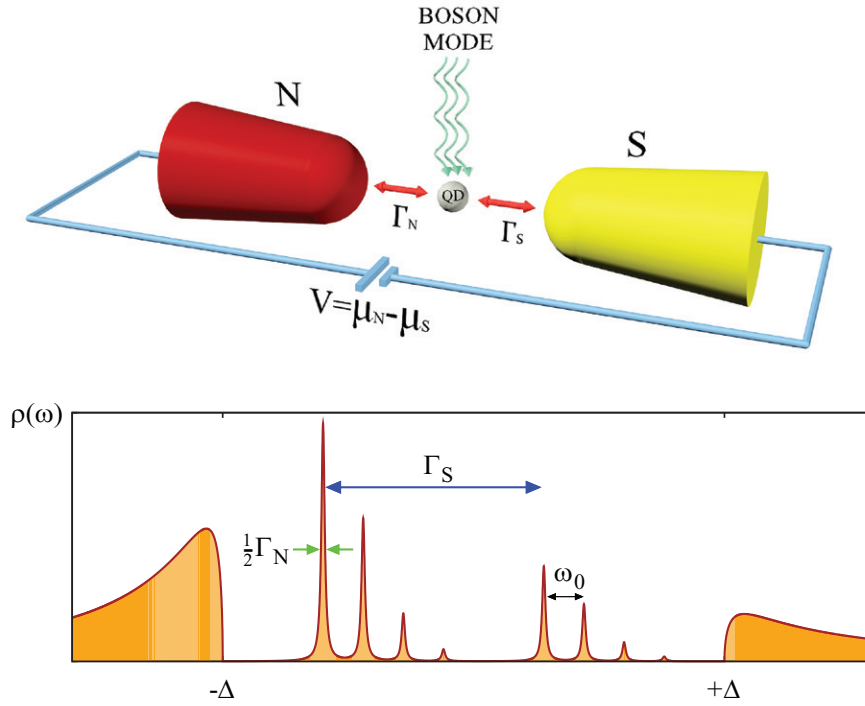
Figure 1. Top panel: scheme of the quantum dot coupled to the metallic (N) and superconducting (S) electrodes and affected by the external boson (vibron or photon) mode. Bottom panel: schematic of the quantum dot spectrum in the limit of weak couplings $\Gamma_S/\Delta < 1$ and $\Gamma_N/\Gamma_S \ll 1$. The low-energy boson mode ω_0 induces two series of the in-gap (Andrev) states, which are split by Γ_S (due to the proximity effect).

the single electron transistor (SET) setup, using e.g. carbon nanotube suspended between some external electrodes as discussed in [10, 12]. Another possibility is the scanning tunneling microscope (STM) structure, where a conducting tip (N) probes a vibrating quantum impurity (QD) hosted in some superconducting (S) medium [34]. In both SET and STM configurations such a boson mode can eventually be related to the ac field.

Previously we have addressed a somewhat different setup in which the bosonic mode affected the subgap Andreev conductance indirectly, through the second (side-attached) quantum dot [35]. That situation would be relevant to complex molecules whose peripheral components (e.g. single atoms weakly coupled to the molecular core) are very susceptible to any vibrational/photonic degrees of freedom. The side-attached quantum dot inherits the bosonic features in a standard way. Through the inter-dot coupling, they are next transmitted to the central dot, giving rise to Fano-type resonances appearing in the normal [36] and anomalous transport channels [35]. The proximity effect merely doubles a number of such signatures. In distinction to our present study, such Fano-type features never cross each other (they do not interfere).

In what follows we introduce the Hamiltonian and discuss the method for treating the bosonic mode. Next, we investigate the bosonic signatures appearing in the QD spectrum and in the subgap Andreev conductance. For the sake of clarity, we focus on the limit $\Gamma_N \ll \omega_0$ whereas the second coupling Γ_S can be arbitrary. We provide an analytical argument explaining the reduced frequency $\omega_0/2$ of the bosonic features in the linear subgap conductance. Moreover, we study the induced in-gap states originating from emission/absorption of boson quanta

and argue that these Andreev states could also enhance the nonlinear subgap conductance at some characteristic values of the source–drain voltage. In the final section we address the correlation effects.

2. Microscopic model

For description of the tunneling scheme (figure 1) we use the single-impurity Anderson model

$$\hat{H} = \hat{H}_N + \hat{H}_S + \hat{H}_{mol} + \hat{H}_T, \qquad (1)$$

where $\hat{H}_{N(S)}$ refers to the normal (superconducting) lead, $\hat{H}_{mol}$ describes the molecular quantum dot (i.e. the localized electrons coupled with the boson mode) and $\hat{H}_T$ is a hybridization between the QD and itinerant electrons. We treat the normal electrode as a free Fermi gas $\hat{H}_N = \sum_{\mathbf{k},\sigma} \xi_{\mathbf{k}N} \hat{c}^\dagger_{\mathbf{k}\sigma N} \hat{c}_{\mathbf{k}\sigma N}$ and describe the superconducting lead by the BCS (Bardeen–Cooper–Schrieffer) Hamiltonian $\hat{H}_S = \sum_{\mathbf{k},\sigma} \xi_{\mathbf{k}S} \hat{c}^\dagger_{\mathbf{k}\sigma S} \hat{c}_{\mathbf{k}\sigma S} - \Delta \sum_{\mathbf{k}} (\hat{c}^\dagger_{\mathbf{k}\uparrow S} \hat{c}^\dagger_{-\mathbf{k}\downarrow S} + \hat{c}_{-\mathbf{k}\downarrow S} \hat{c}_{\mathbf{k}\uparrow S})$. As usual, $\hat{c}^{(\dagger)}_{\mathbf{k}\sigma\beta}$ are the annihilation (creation) operators of the itinerant electrons with spin $\sigma = \uparrow, \downarrow$ and energy $\xi_{\mathbf{k}\beta} = \varepsilon_{\mathbf{k}\beta} - \mu_\beta$ measured with respect to the chemical potential μ_β. The non-equilibrium situation can be driven by the source–drain bias $V = \mu_L - \mu_R$ and/or the temperature difference $T_L \neq T_R$. Thus induced currents qualitatively depend on the hybridization part $\hat{H}_T = \sum_{\mathbf{k},\sigma,\beta} (V_{\mathbf{k}\beta} \hat{d}^\dagger_\sigma \hat{c}_{\mathbf{k}\sigma\beta} + \text{H.c.})$ and on parameters of the molecular quantum dot

$$\hat{H}_{\mathrm{mol}} = \varepsilon \sum_\sigma \hat{n}_{d\sigma}^\dagger + U\hat{n}_{d\uparrow}\hat{n}_{d\downarrow} + \omega_0 \hat{a}^\dagger \hat{a} + \lambda \sum_\sigma \hat{n}_{d\sigma}(\hat{a}^\dagger + \hat{a}).$$
$$(2)$$

In equation (2) we introduce the number operator $\hat{n}_{d\sigma} = \hat{d}_\sigma^\dagger \hat{d}_\sigma$ of the localized electrons with spin σ, and U is the Coulomb potential between opposite-spin electrons. The QD energy level ε can be varied by applying the gate voltage. The bosonic degrees of freedom are described by the operators $\hat{a}^{(\dagger)}$ and the coupling to the QD electrons is denoted by λ. For simplicity we consider a single (i.e. monochromatic) mode ω_0.

3. Interference of Andreev states

In order to determine the effective energy spectrum and the tunneling conductance we have to combine the influence of (i) the electron–boson coupling λ, (ii) the proximity induced on-dot pairing (due to Δ), and (iii) the correlation effects caused by the Coulomb repulsion U. The most reliable method for treating them on an equal footing would be the numerical renormalization group (NRG) approach; however, such a method encounters serious problems when estimating the Andreev transmission. To get some insight we start by neglecting the correlations and study the induced in-gap (Andreev) states. Next, in section 5, we study interplay between the on-dot pairing and the correlations using the superconducting atomic limit solution. The latter part qualitatively reproduces the in-gap spectrum obtained previously by the NRG calculations [24] and extends them to the transport properties that would be important for experimental measurements.

Let us first apply the unitary transformation $e^{\hat{S}}\hat{H}e^{-\hat{S}} = \hat{\tilde{H}}$ to decouple the electron from the boson degrees of freedom. Using the Lang–Firsov generating operator [37],

$$\hat{S} = \frac{\lambda}{\omega_0} \sum_\sigma \hat{n}_{d\sigma}(\hat{a}^\dagger - \hat{a}),$$
$$(3)$$

the molecular Hamiltonian (2) is transformed to

$$\hat{\tilde{H}}_{\mathrm{mol}} = \sum_\sigma \tilde{\varepsilon}\hat{\tilde{d}}_\sigma^\dagger \hat{\tilde{d}}_\sigma + \tilde{U}\hat{\tilde{n}}_{d\downarrow}\hat{\tilde{n}}_{d\uparrow} + \omega_0 \hat{a}^\dagger \hat{a}.$$
$$(4)$$

The energy level is lowered by the polaronic shift $\tilde{\varepsilon} = \varepsilon - \lambda^2/\omega_0$ whereas the effective potential is changed to $\tilde{U} = U - 2\lambda^2/\omega_0$. The transformed boson operators are shifted $\hat{\tilde{a}}^{(\dagger)} = \hat{a}^{(\dagger)} - \frac{\lambda}{\omega_0} \sum_\sigma \hat{d}_\sigma^\dagger \hat{d}_\sigma$ and fermion operators are *dressed* with the polaronic cloud:

$$\hat{\tilde{d}}_\sigma^{(\dagger)} = \hat{d}_\sigma^{(\dagger)}\hat{X}^{(\dagger)}, \qquad \hat{X} = e^{-(\lambda/\omega_0)(\hat{a}^\dagger - \hat{a})}.$$
$$(5)$$

The external reservoirs $\hat{H}_\beta$ are invariant on the unitary transformation (3) but $\hat{X}$ appears in the transformed hybridization term $\hat{H}_T$. For simplicity we shall absorb it into the effective coupling constants defined as $\Gamma_\beta = 2\pi \sum_{\mathbf{k}} |V_{\mathbf{k}\beta}|^2 \langle \hat{X}^\dagger \hat{X}\rangle \delta(\omega - \xi_{\mathbf{k}\beta})$.

To get the effective spectrum we need the single-particle Green's function

$$\boldsymbol{G}_\sigma(\tau_1, \tau_2) = -\mathrm{i}\left\langle \hat{T}_\tau \hat{d}_\sigma(\tau_1)\hat{d}_\sigma^\dagger(\tau_2) \right\rangle_{\hat{H}},$$
$$(6)$$

where $\hat{T}_\tau$ denotes the time-ordering operator. Since the trace is invariant on unitary transformations $\langle ... \rangle_{\hat{H}} = \langle ... \rangle_{\hat{\tilde{H}}}$, it is convenient to compute the statistical averages with respect to $\hat{\tilde{H}}$. In particular, the Green's function (6) is decomposed into the product

$$\boldsymbol{G}_\sigma(\tau_1, \tau_2) = -\mathrm{i}\left\langle \hat{T}_\tau \hat{d}_\sigma(\tau_1)\hat{d}_\sigma^\dagger(\tau_2) \right\rangle_{\hat{\tilde{H}}_{\mathrm{fer}}} \left\langle \hat{T}_\tau \hat{X}(\tau_1)\hat{X}^\dagger(\tau_2) \right\rangle_{\hat{\tilde{H}}_{\mathrm{bos}}} \quad (7)$$

because the fermionic and bosonic degrees of freedom are separated by the Lang–Firsov transformation. The second part can be expressed analytically [7, 38]

$$\langle \hat{T}_\tau \hat{X}(\tau_1)\hat{X}(\tau_2)^\dagger \rangle_{\hat{\tilde{H}}_{\mathrm{bos}}} = \exp\{-(\lambda/\omega_0)^2$$
$$\times [(1 - e^{-\mathrm{i}\omega_0(\tau_1 - \tau_2)})(1 + N_p) + (1 - e^{\mathrm{i}\omega_0(\tau_1 - \tau_2)})N_p]\}, \quad (8)$$

where $N_p = [e^{\beta\omega_0} - 1]^{-1}$ is the Bose–Einstein distribution function. Upon Fourier transforming the effective Green's function (8) can be expressed as

$$\boldsymbol{G}_\sigma(\omega) = \sum_l \boldsymbol{g}_\sigma(\omega - l\omega_0) \ e^{-\left(\lambda\sqrt{1+2N_p}/\omega_0\right)^2}e^{l\beta\omega_0/2}I_l$$
$$\times \left[2\left(\frac{\lambda}{\omega_0}\right)^2 \sqrt{N_p(1 + N_p)}\right], \quad (9)$$

where I_l denotes the modified Bessel functions and $\boldsymbol{g}_\sigma(\tau_1, \tau_2) \equiv -\mathrm{i}\left\langle \hat{T}_\tau \hat{d}_\sigma(\tau_1)\hat{d}_\sigma^\dagger(\tau_2) \right\rangle_{\hat{\tilde{H}}_{\mathrm{fer}}}$. In particular, at zero temperature (9) simplifies to

$$\lim_{T \to 0} \boldsymbol{G}_\sigma(\omega) = \sum_l \boldsymbol{g}_\sigma(\omega - l\omega_0) \ e^{-g} \frac{g^l}{l!} \quad (10)$$

with the adiabatic parameter $g = (\lambda/\omega_0)^2$.

In the same framework we can also compute the anomalous Green's function $\boldsymbol{F}(\tau_1, \tau_2) = -\mathrm{i}\left\langle \hat{T}_\tau \hat{d}_\downarrow^\dagger(\tau_1)\hat{d}_\uparrow^\dagger(\tau_2) \right\rangle_{\hat{H}}$ which has direct influence on the subgap conductance (see section 4). In analogy to (7) we can write down
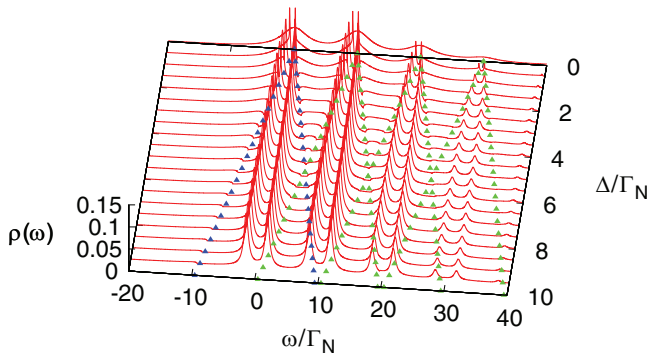
$$\boldsymbol{F}(\tau_1, \tau_2) = -\mathrm{i}\left\langle \hat{T}_\tau \hat{d}_\downarrow^\dagger(\tau_1)\hat{d}_\uparrow^\dagger(\tau_2) \right\rangle_{\hat{\tilde{H}}_{\mathrm{fer}}} \left\langle \hat{T}_\tau \hat{X}^\dagger(\tau_1)\hat{X}^\dagger(\tau_2) \right\rangle_{\hat{\tilde{H}}_{\mathrm{bos}}}. \quad (11)$$

The bosonic part of the anomalous function (11) takes the following form [19]:

$$\left\langle \hat{T}_\tau \hat{X}^\dagger(\tau_1)\hat{X}(\tau_2)^\dagger \right\rangle_{\mathrm{bos}} = \exp\{-(\lambda/\omega_0)^2$$
$$\times [(1 + e^{-\mathrm{i}\omega_0(\tau_1 - \tau_2)})(1 + N_p) + (1 + e^{\mathrm{i}\omega_0(\tau_1 - \tau_2)})N_p]\}. \quad (12)$$

At zero temperature the Fourier transform of (11) is given by

$$\lim_{T \to 0} \boldsymbol{F}(\omega) = \sum_l f(\omega - l\omega_0) \ e^{-g} \frac{(-g)^l}{l!}, \quad (13)$$

Figure 2. Energy spectrum $\rho(\omega)$ of the uncorrelated quantum dot ($\tilde{U} = 0$) obtained at $T = 0$ for $\tilde{\varepsilon} = 0$, $g = 1$, $\omega_0 = 10\Gamma_N$. For increasing Δ the boson peaks split into lower and upper Andreev states and their broadening shrinks to Γ_N. The filled triangles at $l\omega_0 \pm \Delta$ are only as a guide to the eye.

where $\boldsymbol{f}(\omega)$ is the Fourier transform of the fermion part $\boldsymbol{f}(\tau_1, \tau_2) \equiv -\mathrm{i}\langle \hat{T}_\tau \hat{d}^\dagger_\downarrow(\tau_1) \hat{d}^\dagger_\uparrow(\tau_2)\rangle_{\hat{H}_{\mathrm{fer}}}$. We could thus obtain the energy spectrum and study the transport properties (within the Landauer formalism discussed in section 4) if we knew the fermionic parts $\boldsymbol{g}(\omega)$, $\boldsymbol{f}(\omega)$.

We can express these fermionic Green's functions via the Dyson equation:

$$\begin{bmatrix} \boldsymbol{g}(\omega) & \boldsymbol{f}(\omega) \\ \boldsymbol{f}^\star(-\omega) & -\boldsymbol{g}^\star(-\omega) \end{bmatrix}^{-1} = \begin{bmatrix} \omega - \tilde{\varepsilon} & 0 \\ 0 & \omega + \tilde{\varepsilon} \end{bmatrix} - \Sigma_{\mathrm{QD}}(\omega), \qquad (14)$$

where the self-energy matrix Σ_{QD} accounts for the hybridization $\hat{H}_{\mathrm{T}}$ of the quantum dot (4) with external leads and for the correlation effects induced by the effective Coulomb interaction $\tilde{U}$. The first contribution is known exactly $\Sigma_{\mathrm{QD}}^{(U=0)}(\omega) = \sum_{\mathbf{k},\beta} |V_{\mathbf{k}\beta}|^2 g_{\mathbf{k}\beta}(\omega)$, where $g_{\mathbf{k}\beta}(\omega)$ are the Green's functions (in the Nambu representation) of the normal $\beta = N$ and superconducting $\beta = S$ reservoirs. In the wide-band limit approximation it simplifies to the following analytical structure [51]:

$$\Sigma_{\mathrm{QD}}^0(\omega) = -\mathrm{i}\frac{\Gamma_N}{2}\begin{pmatrix} 1 & 0 \\ 0 & 1 \end{pmatrix} - \frac{\Gamma_S}{2}\gamma(\omega)\begin{pmatrix} 1 & \dfrac{\Delta}{\omega} \\ \dfrac{\Delta}{\omega} & 1 \end{pmatrix} \qquad (15)$$

with $\gamma(\omega) = \dfrac{\omega}{\sqrt{\Delta^2 - \omega^2}}$ in a subgap regime $|\omega| < \Delta$ and $\gamma(\omega) = \dfrac{\mathrm{i}\,|\omega|}{\sqrt{\omega^2 - \Delta^2}}$ outside of it.

Figure 2 shows the effective spectral function $\rho(\omega) = -\pi^{-1}\mathrm{Im}\,\boldsymbol{G}(\omega + \mathrm{i}0^+)$ obtained at zero temperature for the intermediate electron-boson coupling $g \sim 1$, neglecting correlation effects. In the normal state (for $\Delta = 0$) the Lorentzian peaks are located at $\omega = \tilde{\varepsilon} + l\omega_0$ (with $l \geqslant 0$) and their broadening is given by $\Gamma_N + \Gamma_S$. In the superconducting state (for $\Delta \neq 0$) these peaks split into lower and upper branches due to the induced on-dot pairing. In the extreme limit $\Delta \gg \Gamma_S$ the self-energy $\Sigma_{\mathrm{QD}}^0(\omega)$ becomes static:
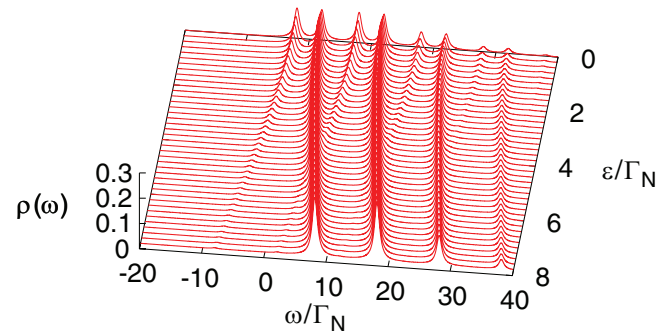
Figure 3. Spectral function $\rho(\omega)$ of the uncorrelated quantum dot obtained for $\omega_0 = 10\Gamma_N$, $g = 1$, $\Gamma_S = 4\Gamma_N$, $T = 0$. The neighboring Andreev states interfere with each other at $\omega = \left(\frac{1}{2} + l\right)\omega_0$ when $\tilde{\varepsilon} \simeq \omega_0/2$.
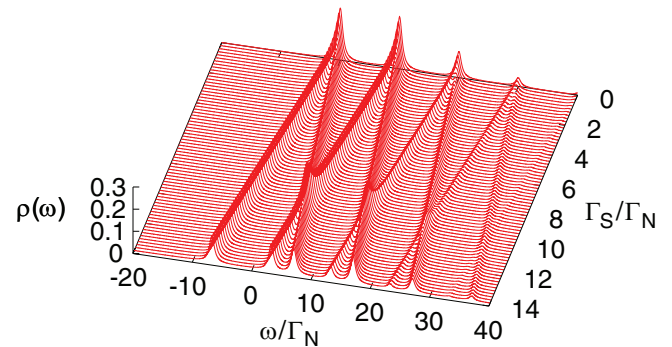
Figure 4. Spectrum of the uncorrelated quantum dot for $\tilde{\varepsilon} = 0$, $g = 1$, $\omega_0 = 10\Gamma_N$, $T = 0$, $\Delta \gg \Gamma_S$. The subgap peaks are overlapping at $\omega = \left(\frac{1}{2} + l\right)\omega_0$ when $\Gamma_S = \omega_0$.

$$\lim_{\Delta \gg \Gamma_S} \Sigma_{\mathrm{QD}}^0(\omega) = -\frac{1}{2}\begin{pmatrix} \mathrm{i}\Gamma_N & \Gamma_S \\ \Gamma_S & \mathrm{i}\Gamma_N \end{pmatrix} \qquad (16)$$

and therefore the quasiparticle energies evolve to $l\omega_0 \pm \sqrt{\tilde{\varepsilon}^2 + (\Gamma_S/2)^2}$ and their broadening shrinks to Γ_N.

Focusing on the superconducting atomic limit (16) we show in figure 3 the subgap bosonic peaks with respect to $\tilde{\varepsilon}$. This QD energy level $\tilde{\varepsilon}$ would be tunable by the gate voltage. In particular, the subgap peaks interfere with each other when $\tilde{\varepsilon} \simeq \omega_0/2$. This can be deduced analytically from the following simple constraint:

$$l\omega_0 + \sqrt{\tilde{\varepsilon}^2 + (\Gamma_S/2)^2} = l'\omega_0 - \sqrt{\tilde{\varepsilon}^2 + (\Gamma_S/2)^2}. \qquad (17)$$

The neighboring peaks ($l' = l + 1$) appear at the same energy when $\omega_0/2 = \sqrt{\tilde{\varepsilon}^2 + (\Gamma_S/2)^2}$. For small coupling Γ_S this situation occurs for $\tilde{\varepsilon} \simeq \frac{1}{2}\omega_0$. This simple reasoning explains why the linear conductance versus the gate voltage is periodically enhanced with the frequency reduced to $\omega_0/2$, as indicated numerically in the earlier studies [21, 25, 29].

Figure 4 shows the subgap spectrum $\rho(\omega)$ as a function of the coupling Γ_S obtained for $\tilde{\varepsilon} = 0$. From equation (17) we conclude that the neighboring Andreev states interfere when $\Gamma_S = \omega_0$ and their crossing points occurs at $\omega = \left(\frac{1}{2} + l\right)\omega_0$. For
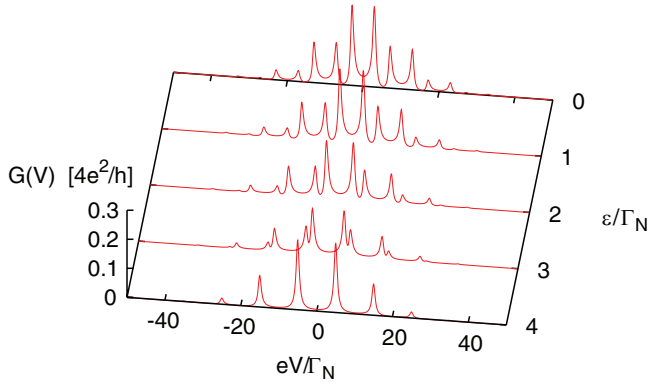
Figure 5. The differential Andreev conductance $G_A(V)$ versus the source-drain voltage V and the QD level ε (tunable by the gate voltage). The results are obtained for the uncorrelated dot at $T = 0$ using $g = 1$, $\Gamma_S/\Gamma_N = 6$, $\omega_0/\Gamma_N = 10$ and $\Delta \gg \Gamma_S$.

$g = 1$ we observe four such crossings, but for stronger couplings g the number of the subgap peaks increases.

4. Andreev conductance

Under nonequilibrium conditions the charge current is transmitted at small bias $|eV| < \Delta$ only via the Andreev scattering. This anomalous transport channel occurs when electrons from the metallic lead are converted into Cooper pairs in the superconducting electrode, reflecting the holes back to the normal electrode. The resulting charge current $I_A(V)$ can be expressed by the following Landauer-type formula [39, 40]:

$$I_A(V) = \frac{2e}{h} \int d\omega \, T_A(\omega)[f_{FD}(\omega - eV) - f_{FD}(\omega + eV)], \quad (18)$$

where $f_{FD}(\omega) = [e^{\omega/k_B T} + 1]^{-1}$ is the Fermi–Dirac function and the Andreev transmittance $T_A(\omega)$ depends on the anomalous Green's function (11)

$$T_A(\omega) = \Gamma_N^2 \, |F(\omega)|^2. \quad (19)$$

Optimal conditions for this transmittance (19) occur near subgap quasiparticle states. We thus expect a series of the subgap transmittance enhancements due to emission/absorption of bosonic quanta. We remark that $T_A(-\omega) = T_A(\omega)$ implies the Andreev conductance $G_A(V) = \frac{\partial I_A(V)}{\partial V}$ to be an even function with respect to the source-drain bias V.

In figure 5 we plot the subgap conductance as a function of V for the uncorrelated quantum dot $\tilde{U} = 0$. We clearly notice several maxima whenever V coincides with the quasiparticle energies $\pm\sqrt{\tilde{\varepsilon}^2 + (\Gamma_S/2)^2} \pm l\omega_0$. They eventually overlap when the condition (17) is satisfied. In particular, for $\Gamma_S = 6\Gamma_N$ and $\omega_0 = 10\Gamma_N$ the neighboring Andreev peaks interfere when $\tilde{\varepsilon} = 4\Gamma_N$ and the resulting enhancements appear at $|eV| = \omega_0(1/2 + l)$.

5. Correlation effects

In experimental realizations of quantum dots (e.g. self-assembled InAs islands [41], carbon nanotubes [42, 43], or semiconducting

nanowires [44, 45]) coupled to the superconducting leads, the energy gap Δ was much smaller than the repulsion potential U. Under such circumstances the correlations affect the subgap Andreev spectroscopy predominantly via the singlet–doublet quantum phase transition [46]. At sufficiently low temperatures in the doublet configuration one may eventually also encounter the Kondo-type correlations. This issue has been pioneered in the early study by Fazio with Raimondi [47] and has been extensively addressed by many other authors using various methods [48–52]. In this paper we consider the strongly asymmetric coupling $\Gamma_N \ll \Gamma_S$ and focus on the deep subgap regime $\Gamma_{N,S} \ll \Delta$; therefore the Kondo effect is rather negligible.

The spectrum of the vibrating quantum dot near the singlet–doublet transition has been previously addressed by the NRG technique [24]. We revisit the same issue here, determining the differential Andreev conductance (difficult to calculate in the NRG method), because this quantity would be of interest for experimentalists. For the sake of simplicity, we analyze the correlation effects in the superconducting atomic limit $\Delta \gg \Gamma_S$. Hamiltonian of the molecular quantum dot (4) should be then supplemented by the pairing terms $\frac{1}{2}\Gamma_S(\hat{d}_\uparrow^\dagger \hat{d}_\downarrow^\dagger + \hat{d}_\downarrow \hat{d}_\uparrow)$ originating from the static off-diagonal parts of the self-energy matrix (16).

In the absence of the boson field (i.e. for $\lambda = 0$) the exact solution of such problem has been discussed by a number of authors (e.g. see the references cited in [53]). The effective quasiparticle energies are given by $\pm U/2 \pm E_d$, where $E_d = \sqrt{(\varepsilon + U/2)^2 + (\Gamma_S/2)^2}$. In the realistic situations only two branches $\pm(U/2 - E_d)$ appear in the subgap regime, whereas the other high-energy states $\pm(U/2 + E_d)$ overlap with a continuum beyond the gap. The quantum phase transition (QPT) from the singlet $u|0\rangle + v|\uparrow\downarrow\rangle$ to doublet $|\sigma\rangle$ configuration occurs at $U/2 = E_d$ [46]. To estimate the Andreev conductance we use the off-diagonal Green's function $f(\omega)$ [46, 53], restricting to its subgap part:

$$f_{sub}(\omega) \simeq \frac{\alpha \, uv}{\omega + \frac{i\Gamma_N}{2} - \left(\frac{U}{2} - E_d\right)} - \frac{\alpha \, uv}{\omega + \frac{i\Gamma_N}{2} + \left(\frac{U}{2} - E_d\right)} \quad (20)$$

with the usual BCS coefficient $uv = \Gamma_S/4E_d$ and the spectral weight $\alpha = \left[\exp\left(\frac{U}{2k_B T}\right) + \exp\left(\frac{E_d}{k_B T}\right)\right]/\mathcal{Z}$, where $\mathcal{Z} = 2\exp\left(\frac{U}{2k_B T}\right) + \exp\left(\frac{-E_d}{k_B T}\right) + \exp\left(\frac{E_d}{k_B T}\right)$. The missing part of the spectral weight $1 - \alpha$ belongs to the high-energy states (outside the gap). At zero temperature this subgap weight changes abruptly from $\alpha = 1$ (in the singlet state when $U/2 < E_d$) to $\alpha = 0.5$ (in the doublet state when $U/2 > E_d$).

Figure 6 shows the Andreev conductance obtained for the half-filled quantum dot $\varepsilon = -U/2$ (where QPT is at $U = \Gamma_S$) in absence of the electron-boson coupling. The subgap conductance is characterized by two maxima around $|eV| = U/2 - E_d$. At the very QPT, these quasiparticle contributions cancel each other (see the thick red line in figure 6) because the anomalous Green's function (20) vanishes at the QPT.

We can easily extend the superconducting atomic limit solution to the case $g \neq 0$. The unitary transformation (3) implies $\varepsilon \rightarrow \tilde{\varepsilon}$, $U \rightarrow \tilde{U}$, so following the considerations (11)–(16), we can obtain the off-diagonal Green's function. At zero temperature we find
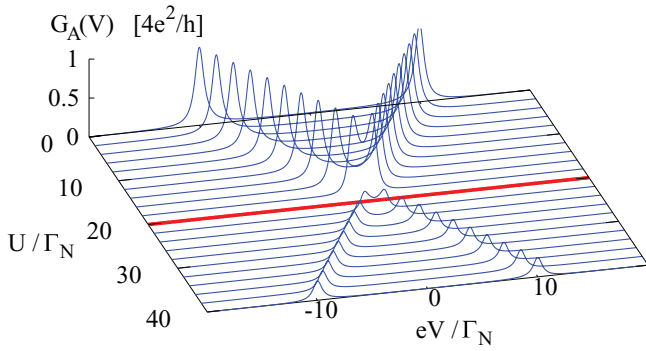
Figure 6. The differential Andreev conductance $G_A(V)$ versus the Coulomb potential U and bias V obtained in the superconducting atomic limit $\Delta \gg \Gamma_S$ for $T = 0$, $\Gamma_S/\Gamma_N = 20$ in absence of the boson mode $g = 0$. The thick (red) line indicates the QPT at $U = \Gamma_S$.
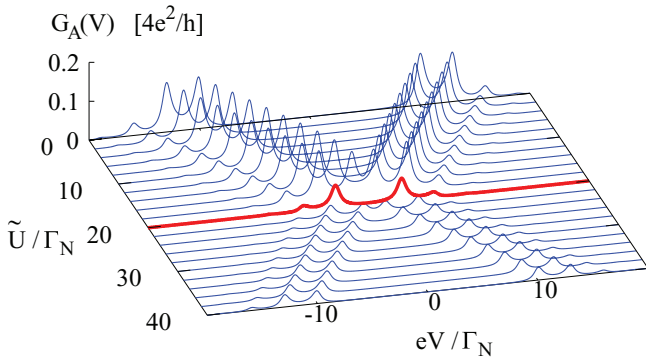
Figure 7. The subgap Andreev conductance $G_A(V)$ as a function of the Coulomb potential $\tilde{U}$ and voltage V obtained for $g = 1$, $\omega_0/\Gamma_N = 10$ and the same model parameters as in figure 6.

$$F_{\text{sub}}(\omega) \simeq e^{-g} \sum_{l=0}^{\infty} \frac{(-g)^l}{l!} \left\{ \frac{\alpha\ uv}{\omega + \frac{i\Gamma_N}{2} - \left(\frac{\tilde{U}}{2} - E_d\right) + s\ l\omega_0} \right.$$
$$\left. - \frac{\alpha\ uv}{\omega + \frac{i\Gamma_N}{2} + \left(\frac{\tilde{U}}{2} - E_d\right) - s\ l\omega_0} \right\} \tag{21}$$

with $s \equiv \text{sign}\left(\frac{\tilde{U}}{2} - E_d\right)$. Figure 7 shows the Andreev conductance obtained for the half-filled quantum dot using $g = 1$, $\omega_0/\Gamma_N = 10$, $\Gamma_S/\Gamma_N = 20$, and $T = 0$. The in-gap Andreev states give rise to two subgap branches, similar to what has been reported in the spectral function in the NRG calculations [24]. The differential Andreev conductance shows the maxima at $|eV| = |\tilde{U}/2 - E_d| + l\omega_0$. Their spectral weights depend on l via equation (21) appearing in the Andreev transmittance (19) and are sensitive to the ratio U/Γ_S.

6. Summary

We have investigated the subgap spectrum and transport properties of the quantum dot coupled between metallic and superconducting electrodes in the presence of an external boson mode ω_0. We have shown that the in-gap Andreev states eventually interfere: (a) by applying the gate voltage (upon varying ε) or (b) due to the strong correlations (via the singlet–doublet quantum phase transition). We have explored their signatures in the measurable subgap transport. The tunneling conductance of such multilevel 'molecule' reveals the characteristic enhancements that appear with the reduced frequency $\omega_0/2$ as a function of the gate voltage. We have explained this anomalous behavior analytically (see equation (17) and the discussion that follows it). Furthermore, we have also predicted enhancements of Andreev conductance beyond the linear response regime at specific values of the source–drain bias V (figure 5). We have shown that the differential Andreev conductance strongly depends on the correlations, especially near the singlet–doublet transition (figure 7). Summarizing, we conclude that the external boson modes can lead to substantial enhancements of Andreev conductance due to emission/absorption of bosonic quanta. Such features could be experimentally observed using the low-energy vibrational modes or the ac fields.

References

[1] Platero G and Aguado R 2004 *Phys. Rep.* **395** 1
[2] Mitra A, Aleiner I and Millis A J 2004 *Phys. Rev.* B **69** 245302
[3] Galperin M, Ratner M A and Nitzan A 2007 *J. Phys.: Condens. Matter* **19** 103201
[4] Viljas J K, Cuevas J C, Pauly F and Häfner M 2005 *Phys. Rev.* B **72** 245415
[5] Koch J and von Oppen F 2005 *Phys. Rev. Lett.* **94** 206804
[6] Koch J, von Oppen F and Andreev A V 2006 *Phys. Rev.* B **74** 2054368
[7] Fransson J 2010 *Non-Equilibrium Nano-Physics: A Many-Body Approach* (Berlin: Springer) pp 107–15
[8] Agrait N, Levy Yeyati A and Ruitenbeek J M 2003 *Phys. Rep.* **377** 81
[9] Pasupathy A N *et al* 2005 *NanoLetters* **5** 203
[10] Sapmaz S, Jarillo-Herrero P, Blanter Ya M, Dekker C and van der Zant H S J 2006 *Phys. Rev. Lett.* **96** 026801
[11] Beebe J M, Kim B S, Gadzuk J W, Frisbie C D and Kushmerick J G 2006 *Phys. Rev. Lett.* **97** 026801
[12] Leturcq R, Stampfer C, Inderbitzin K, Durrer L, Hierold C, Mariani E, Schultz M G, von Oppen F and Ensslin K 2009 *Nat. Phys.* **5** 327
[13] Zazunov A, Egger R, Mora C and Martin T 2006 *Phys. Rev.* B **73** 214501
[14] Jarillo-Herrero P, van Dam J A and Kouwenhoven L P 2006 *Nature* **439** 953
[15] Cleuziou J-P, Wernsdorfer W, Bouchiat V, Ondarcuhu T and Monthioux M 2006 *Nat. Nanotechnol.* **1** 53
[16] Sköldberg J, Löfwander T, Shumeiko V S and Fogelström M 2008 *Phys. Rev. Lett.* **101** 087002
[17] Pillet J-D, Quay C H L, Morfin P, Bena C, Levy Yeyati A and Joyez P 2010 *Nat. Phys.* **6** 965

[18] Fransson J, Balatsky A V and Zhu J-X 2010 *Phys. Rev.* B **81** 155440
[19] Wu B H, Cao J C and Timm C 2012 *Phys. Rev.* B **86** 035406
[20] Stadler P, Holmqvist C and Belzig W 2013 *Phys. Rev.* B **88** 104512
[21] Cho S Y, Kang K and Ryu C-M 1999 *Phys. Rev.* B **60** 16874
[22] Zhang P and Li Y-X 2009 *J. Phys.: Condens. Matter* **21** 095602
[23] Bai L, Zhang Z-Z and Jiang J 2011 *Phys. Lett.* A **375** 661
[24] Golež D, Bonča J and Žitko R 2012 *Phys. Rev.* B **86** 085142
[25] Zhang S N, Pei W, Fang T F and Sun Q F 2012 *Phys. Rev.* B **86** 104513
[26] Bocian K and Rudziński W 2014 *Acta Phys. Polon.* A **126** 374
[27] Song H-Y and Zhou S-P 2008 *Phys. Lett.* A **372** 6773
[28] Albrecht K F, Soller H, Mühlbacher L and Komnik A 2013 *Physica* E **54** 15
[29] Wang Q, Xie H, Jiao H and Nie Y-H 2013 *Europhys. Lett.* **101** 47008
[30] Faivre T, Golubev D S and Pekola J P 2015 *Appl. Phys. Lett.* **106** 182602
[31] Mazza F, Valentini S, Bosisio R, Benenti G, Giovannetti V, Fazio R and Tadddei F 2015 *Phys. Rev.* B **91** 245435
[32] Hofstetter L, Csonka S, Nyg J and Schönenberger C 2009 *Nature* **461** 960
[33] Herrmann L G, Portier F, Roche P, Levy Yeyati A, Kontos and Strunk C 2010 *Phys. Rev. Lett.* **104** 026801
[34] Balatsky A V, Vekhter I and Zhu J-X 2006 *Rev. Mod. Phys.* **78** 373
[35] Barański J and Domański T 2015 *Chin. Phys.* B **24** 017304
[36] Žitko R 2010 *Phys. Rev.* B **81** 115316
[37] Lang I G and Firsov Y A 1963 *Sov. Phys.—JETP* **16** 1301
[38] Mahan G D 2000 *Many-Particle Physics* (New York: Academic) pp 218–28
[39] Sun Q-F, Wang J and Lin T-H 1999 *Phys. Rev.* B **59** 3831
[40] Krawiec M and Wysokiński K I 2004 *Supercond. Sci. Technol.* **17** 103
[41] Deacon R S, Tanaka Y, Oiwa A, Sakano R, Yoshida K, Shibata K, Hirakawa K and Tarucha S 2010 *Phys. Rev.* B **81** 121308
[42] Pillet J D, Joyez P, Žitko R and Goffman F M 2013 *Phys. Rev.* B **88** 045101
[43] Schindele J, Baumgartner A, Maurand R, Weiss M and Schönenberger C 2014 *Phys. Rev.* B **89** 045422
[44] Lee E J H, Jiang X, Aguado R, Katsaros G, Lieber C M and De Franceschi S 2012 *Phys. Rev. Lett.* **109** 186802
[45] Lee E J H, Jiang X, Houzet M, Aguado R, Lieber Ch M and De Franceschi S 2014 *Nat. Nanotechnol.* **9** 79
[46] Bauer J, Oguri A and Hewson A C 2008 *J. Phys.: Condens. Matter* **19** 486211
[47] Fazio R and Raimondi R 1998 *Phys. Rev. Lett.* **80** 2913
[48] Domański T and Donabidowicz A 2008 *Phys. Rev.* B **78** 073105
[49] Koerting V Andersen B M, Flensberg K and Paaske J 2010 *Phys. Rev.* B **82** 245108
[50] Martín-Rodero A and Levy Yeyati A 2011 *Adv. Phys.* **60** 899
[51] Yamada Y, Tanaka Y and N.Kawakami N 2011 *Phys. Rev.* B **84** 075484
[52] Žitko R, Lim J S, López R and Aguado R 2015 *Phys. Rev.* B **91** 045441
[53] Barański J and Domański T 2013 *J. Phys.: Condens. Matter* **25** 435305